1592 *Macromolecules* **2010**, *43*, 1592–1601
DOI: 10.1021/ma902101n

Macromolecules
ARTICLE

Characteristic Length Scales and Radial Monomer Density Profiles of Molecular Bottle-Brushes: Simulation and Experiment

Hsiao-Ping Hsu,* Wolfgang Paul, Silke Rathgeber, and Kurt Binder

Institut für Physik, Johannes Gutenberg-Universität Mainz D-55099 Mainz, Staudinger Weg 7, Germany

Received September 23, 2009; Revised Manuscript Received December 8, 2009

ABSTRACT: Extensive Monte Carlo simulations are presented for bottle-brush polymers under good solvent conditions, using the bond fluctuation model on the simple cubic lattice. Varying the backbone length (from $N_b = 67$ to $N_b = 259$ effective monomers) as well as the side chain length (from $N = 6$ to $N = 48$), for a physically reasonable grafting density of one chain per backbone monomer, we find that the structure factor describing the total scattering from the bottle-brush provides an almost perfect match for some combinations of (N_b, N) to experimental data of Rathgeber et al. [*J. Chem. Phys.* **2005**, *122*, 124904], when we adjust the length scale of the simulation to reproduce the experimental gyration radius of the bottle-brush. While in the experiment other length scales (gyration radius of side chains, backbone persistence length, scale characterizing the radial monomer density profile in the plane normal to the backbone) can be extracted only via fitting to a complicated and approximate theoretical expression derived by Pedersen and Schurtenberger, all these properties can be extracted from the simulation directly. In this way, quantitatively more reliable estimates for the persistence length and side chain gyration radius of the experimental systems can be extracted. In particular, we show that the popular assumption of a Gaussian radial monomer density profile is inaccurate, in the very good solvent regime studied by the simulation, and show that alternative forms based on scaling theory work better. We also show that the persistence length of the bottle brush in the simulation depends systematically on the backbone length and not only on the side chain length. For the cases where an explicit comparison with the experimental results (based on their evaluation within the Pedersen−Schurtenberger model) is possible, simulation and experiment are consistent with each other and some of the (rather minor) differences between simulation and experiment can be attributed to the weaker strength of excluded volume in the latter. Thus, we show that by suitable mapping between simulation and experiment on length scales of the local concentration fluctuations (here < 2 nm) the analysis of experimental data can be systematically refined.

1. Introduction and Overview

Molecular bottle-brushes consist of a long polymer chain serving as a "backbone" on which flexible linear side chains are densely grafted.[1−14] Such macromolecules have found abiding recent interest, both from the point of view of the chemical synthesis and experimental characterization (see e.g. ref 2 and 3 for beautiful reviews, and also refs 9−11 for a more complete account of the pertinent literature) and from the point of view of the theoretical modeling.[15−44] Part of this interest stems from the possibilities to use these cylindrical brushes as building blocks in supramolecular assemblies,[1,2] or exploit their stimuli-response character to changes in temperature, pH value of the solution, etc., for possible applications as actuators and sensors,[45,46] or explore the unusual lubrication properties of biological bottle-brushes such as aggrecan molecules in human joints,[47,48] but all these aspects are not our focus here.

We rather focus on the unusual conformational properties[41,43,49] of these complex macromolecules, which are due to the competition of many (mesoscopic) length scales in the structure, such as the stiffness of the backbone (which is not ruled by the chemistry of the main chain alone, but is strongly influenced by the grafting density and length of the side chains), the gyration radius of the side chains, and the shape and size of the molecular bottle-brush as a whole. While for simple linear chains under good solvent conditions there exists a simple scaling relation between the degree of polymerization and the total gyration radius,[50−52] involving the Flory−deGennes exponent $\nu \approx 0.588$, and also the distribution function of distances $P_{ij}(r)$ between monomers, with labels i, j along the chain is rather accurately known, the scaling description of bottle-brush polymers is much more complicated. One does expect a scaling law for the end-to-end distance of the backbone

$$\langle R_{e,b}^2 \rangle = 2\ell_b \tilde{\ell_p}(\sigma, N) N_b^{2\nu} \tag{1}$$

where ℓ_b is the distance between two subsequent monomers of the N_b monomers of the backbone, and $\tilde{\ell_p}(\sigma, N)$ is another length which can be taken as one of the measures for the "persistence length" of the backbone. Understanding how $\tilde{\ell_p}(\sigma, N)$ depends on the grafting density σ and chain length N of the side chains is one of the still debated issues in the theory of bottle-brushes.[15−40] Also experiments have made considerable efforts to estimate the persistence length of bottle-brushes.[1−14] However, as we shall discuss below, under good solvent conditions some of the definitions for the persistence length (as a measure of intrinsic stiffness of a chain) are somewhat ill-defined, and different definitions yield results that are not mutually consistent, as has been already noted in the literature recently.[39,40]

Similarly, the linear dimensions of the side chains also are under discussion (a recent review has been given by Hsu et al.).[41] For very large N one expects that the side chains are considerably stretched in the direction perpendicular to the backbone, so their root-mean-square end-to-end distance is[41]

$$\langle R_{e,s}^2 \rangle^{1/2} \propto \ell_s (\sigma \ell_b)^{(1-\nu)/(1+\nu)} N^{2\nu/(1+\nu)} \approx \ell_s (\sigma \ell_b)^{0.259} N^{0.74} \tag{2}$$

*Corresponding author.

 Published on Web 01/07/2010

which implies that the chain is almost as much stretched as if it were confined to the two-dimensional plane normal to the backbone. In eq 2, ℓ_s is the distance between monomers along the side chains. In addition, for an intermediate range of distances r a power-law decay of the monomer density around the backbone is predicted.[18,19,21,41] ($R_{e,s}$ is the and-to-end distance of a side chain, see eq 5 below.)

$$\rho(r) \propto \ell_s^{-3}[(r/\ell_s)/(\sigma l_b)]^{-(3\nu-1)/(2\nu)} \approx \ell_s^{-3}[r/(\sigma \ell_s \ell_b)]^{-0.65}, \quad \ell_s \ll r \ll \langle R_{e,s}^2 \rangle^{1/2} \tag{3}$$

However, the practical relevance of the scaling limit described by eqs 2 and 3 is rather unclear: simulations[40,41] indicate that one needs very large N and/or large σ to be able to access this scaling limit, and this limit probably does neither apply to the available simulations[40,41] nor the available experiments.[9−14] A further caveat that needs to be made is that very close to the backbone the density of the side chain monomers for large σ will be rather high, due to the monomers of side chains connected to their grafting sites. This region clearly is excluded from the scaling description (for this reason, the condition $\ell_s \ll r$ in eq 3 was noted). A problem that also is not fully understood is the anisotropic character of the screening of the excluded volume interactions in the scaling regime[41] (directions parallel and perpendicular to the backbone are not equivalent). While scaling descriptions in terms of "blobs" are straightforward both for star polymers (which have full spherical symmetry) and for polymer brushes on flat substrates,[53] they are problematic for bottle-brushes even in the simplified limit of straight rigid backbones.[41]

Thus, for the analysis of experiments simple ad-hoc assumptions for the radial density profile $\rho(r)$ have been made, such as a Gaussian profile[9−11]

$$\rho(r) \propto \exp(-r^2/\langle R_{g,cs}^2 \rangle) \tag{4}$$

where the mean square cross-section radius of gyration is defined as

$$\langle R_{g,cs}^2 \rangle = 2\pi \int_0^\infty r\, \mathrm{d}r\, \rho(r) r^2 \tag{5}$$

assuming a normalization

$$2\pi \int_0^\infty r\, \mathrm{d}r\, \rho(r) = 1 \tag{6}$$

Alternatively, a power law decay was used[9]

$$\rho(r) = \begin{cases} 1, & r \le R_c \\ \alpha r^{-x}\{1+\exp[(r-R_s)/\sigma_s]\}^{-1}, & r > R_c \end{cases} \tag{7}$$

with the constant α fixed by normalization, eq 6, and R_c, R_s, σ_s, x being fit parameters. The Fermi function serves as a cutoff function at large r only. Still a different formula was suggested in the context of simulations for bottle-brush polymers with rigid backbones,[43]

$$\rho(r) = \frac{\alpha'}{1+(r/r_1)^{(3\nu-1)/2\nu}} \exp[-(r/r_2)^x] \tag{8}$$

with the constant α' fixed by eq 6, and with r_1 r_2 and the exponent x being fit parameters. Note that eq 8 reduces to eq 3 if $r_1 \ll r \ll r_2$ (we expect r_1 to be of the order ℓ_s, and r_2 to be of the order $\langle R_{g,cs}^2 \rangle^{1/2}$).

While in the simulations of bottle-brush polymers the direct determination of $\rho(r)$ is straightforward for the case of straight rigid backbones, and also is still possible almost without any ambiguity in the case of flexible backbones, provided the persistence length is sufficiently large[49] {i.e., $\ell_p \ge \langle R_{g,cs}^2 \rangle^{1/2}$} existing experiments have inferred $\rho(r)$ and $\langle R_{g,cs}^2 \rangle$ rather indirectly and approximately from scattering data. While the small-angle scattering of neutrons or electromagnetic radiation from bottle-brush polymers in dilute solution yields precise information on the mean square gyration radius of the total bottle-brush polymer ($\langle R_{g,bb}^2 \rangle$), since the structure factor $S(q)$ for small wavenumber q can be expanded as

$$S(q) = S(q=0)\left[1 - \frac{1}{3}q^2 \langle R_{g,bb}^2 \rangle + \ldots\right] \tag{9}$$

a similarly direct estimation of $\rho(r)$ and $R_{g,cs}^2$ is not possible. Thus, the standard procedure to analyze the scattering data from bottle-brush polymers[9−14] is based on a decoupling approximation[54,55] which seems to describe well the scattering from worm-like micelles[55]

$$S(q) \approx S_{cs}(q) S_b(q) \tag{10}$$

where the cross-section form factor $S_{cs}(q)$ is approximated in terms of the monomer density distribution $\rho(r)$ as[55,56]

$$S_{cs}(q) = \left[2\pi \int_0^\infty \rho(r) J_0(qr) r\, \mathrm{d}r\right]^2 \tag{11}$$

$J_0(qr)$ being the Bessel function of the first kind of zeroth order. The scattering due to the backbone $S_b(q)$ is written as[55]

$$S_b(q) = [1-\chi(q)] S_{\mathrm{chain}}(q) + \chi(q) S_{\mathrm{rod}}(q) \tag{12}$$

in order to describe a possible crossover from the structure of a straight rod (which has the structure factor S_{rod}) to that of a flexible self-avoiding chain (which has the structure factor S_{chain}), and $\chi(q)$ is a function with the behavior $\chi(q) \to 0$ for $q\ell_p \to 0$ while $\chi(q) \to 1$ for $q\ell_p$ large.[55] However, even in the rigid rod limit, where[56]

$$S_b(q) = \frac{2}{q}\int_0^{qL_b} \frac{\sin t}{t}\, \mathrm{d}t - 4\frac{\sin^2(qL_b/2)}{q^2 L_b} \tag{13}$$

$L_b = N_b \ell_b$ being the backbone length, and any uncertainty about the correct choice of $\chi(q)$ does not enter, the decoupling approximation inherent in eqs 10, 11 was found to be rather inaccurate for bottle-brushes under good solvent conditions.[43] Density fluctuations on small and intermediate length scales are not fully included when eqs 10 and 11 are used, and hence the scattering at large q is not properly described. This finding raises doubt on the conclusions drawn from eq 10, 11 on the quantitative values of $\langle R_{g,cs}^2 \rangle$ (eq 5) and the form of the density profile $\rho(r)$, inferred from the data via eqs 10 and 11. Similar conclusions were already reached by Yethiraj[40] in his simulation study of an off-lattice model of bottle-brushes with flexible backbones.

For controlling the function of bottle-brush polymers in various applications (e.g., refs 45−48), an accurate characterization of their structure is clearly desirable. Therefore, we reconsider the analysis of scattering data, such as those presented by Rathgeber et al.,[9] using large-scale simulations carried out for the bond fluctuation model[57−59] to guide this reanalysis. We note that many previous simulations of bottle-brush polymers have been performed[10,21,27,30−35,40] but our studies stand out by very good statistical accuracy for rather large macromolecules (up to a maximum number of $N_b N = 12432$ monomers in the side chains, $N_b = 259$, $N = 48$). This advance was possible by the use of a new more efficient algorithm (inspired by a previous similar algorithm used for the simulation of dense melts).[60] A similar range of sizes and a similar accuracy could previously only be reached for bottle-brushes with rigid backbones where the

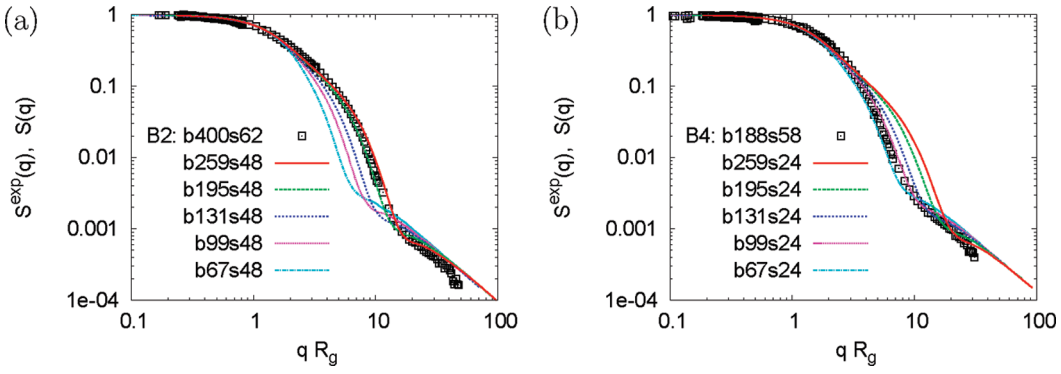

Figure 1. (a) Structure factor of Rathgeber et al.[9] for $N_b^{exp} = 400$, $N^{exp} = 62$ plotted vs qR_g ($R_g = (\langle R_{g,bb}^2 \rangle)^{1/2}$) and comparing to simulated structure factors for $N = 48$ and several backbone lengths N_b, as indicated. Both $S(q)$ and $S^{exp}(q)$ are normalized to unity for $q \to 0$. Using the experimental[9] total gyration radius $(\langle R_{g,bb}^2 \rangle^{exp})^{1/2} = 30.5$ nm and adjusting it to the simulation value $\langle R_{g,bb}^2 \rangle^{1/2} = 115.8$ (lattice spacings), the conversion factor for the length scale 1 nm ≈3.79 lattice spacings is obtained. (b) Same as (a) but for $N_b^{exp} = 188$, $N^{exp} = 58$, and simulated structure factors for $N = 24$ and several backbone lengths. In this case the length scale conversion is 1 nm ≈2.235 lattice spacings.

PERM algorithm[61] is applicable[41−43] and in Yethiraj's study[40] of a tangent hard sphere model.

Figure 1 illustrates the starting point of our analysis: from the data presented by Rathgeber et al.[9] for a range of bottle-brush polymers with different backbone chain length (N_b^{exp}), and side chain length (N^{exp}), we can identify a number of choices (N_b^{exp}, N^{exp}) where a quantitatively accurate mapping of the experimental structure factor $S^{exp}(q)$ on the simulated structure factor $S(q)$, for carefully chosen pairs of parameters (N_b,N), is possible. Here we use a superscript "exp" to distinguish the real experimental data from their simulation counterparts. Thus, apart from suitable adjustment of N_b and N the length scale of the simulation (i.e.; the lattice spacing) is adjusted to physical units, which simply is done by requiring

$$\langle R_{g,bb}^2 \rangle^{exp} = \langle R_{g,bb}^2 \rangle \tag{14}$$

since $\langle R_{g,bb}^2 \rangle^{exp}$ can be obtained from $S^{exp}(q)$ *without invoking the decoupling*, eq 10, which we wish to thoroughly test. From Figure 1 we see that in case (a) a good fit of $S(q)$ over the entire q range (up to $q \approx 1$ nm^{-1}) is obtained for $N = 259$ and in case (b) for $N_b = 99$. Given this agreement, the simulation can predict $\rho(r)$ and $\langle R_{g,cs}^2 \rangle$ on an absolute scale for these systems, and hence we can compare quantitatively to the corresponding estimates extracted from the experiment.[9] In addition, from the simulations we can calculate directly $S_{cs}(q)$ and $S_b(q)$ and test all the steps of the approximations, eqs 10−12, for experimentally relevant cases. Note that both experiment and simulation have used grafting density $\sigma = 1$ (i.e., one side chain per backbone monomer).

The outline of the remainder of the paper is as follows. In the next section we briefly describe first the simulation model and characterize its properties. In the third section, the comparison between experiment and simulation is presented in more detail, and the physical significance of the conversion factors for chain lengths and length scales in real space, from the simulation to the experiment, will be critically evaluated, emphasizing that unique mappings between simulation and experiment cannot be expected, due to the inherent arbitrariness of coarse-graining when one converts n^{exp} monomers of a real chain into n monomers of a model chain. In addition, for the not so long chain lengths available in both experiment and simulation it matters that the "strength" of the excluded volume interactions[50−52] in the experiment may be somewhat weaker than in the simulation (for the bond fluctuation model the scaling $\langle R_g^2 \rangle \propto N^{2\nu}$ for isolated chains is reached[59] already for smaller N than what is typically achieved in experiments).[52]

2. The Simulation Model and Its Properties

As is well-known, the bond fluctuation model of flexible polymers[57−59] describes a macromolecule as a chain of effective monomers on a simple cubic lattice, such that each effective monomer blocks all eight corners of an elementary cube of the lattice from further occupation. Two monomers along a chain are connected by a bond vector $\vec{\ell}$ chosen from the set {(±2, 0, 0), (±2, ±1, 0), (±2, ±1, ±1), (±2, ±2, ±1), (±3, 0, 0), (±3, ±1, 0)}, including also all permutations. While traditionally configurations are relaxed by a Monte Carlo algorithm where a monomer of the chain is chosen at random and moved along one of the six randomly chosen lattice directions, Wittmer et al.[60] showed that a much faster equilibration results if one allows attempts to move a monomer to one of the 26 nearest and next nearest neighbor sites surrounding a monomer ("L 26" move).[60] Of course, any attempted Monte Carlo move is accepted only if it does not violate excluded volume and bond length constraints.

We generalize this standard model for linear polymers to bottle-brush architecture, by adding side chains at regular spacings $1/\sigma$ (which must be integer) to the backbone chain, and furthermore add one more monomer at each chain end of the backbone. Thus, the number of monomers of the backbone N_b is related to the number of side chains n_c via

$$N_b = [(n_c - 1)/\sigma + 1] + 2 \tag{15}$$

and the total number of monomers of the bottle-brush then is $N_{tot} = N_b + n_c N$. However, in order to maintain a close similarity to the experimental situation, where about one side chain per backbone monomer was grafted, here only data for $\sigma = 1$ will be shown, deferring an analysis of less dense bottle-brushes to a future publication.[63]

In order to provide an efficient equilibration of the bottle-brush conformation, in addition to the local "L 26" move[60] also pivot moves[62] are used. Two types of moves are attempted: (i) a monomer on the backbone is chosen randomly and the short part of the bottle-brush polymer is transformed by randomly choosing one of the 48 symmetry operations (no change; rotations by 90^o and 180^o; reflections and inversions). (ii) A monomer is chosen randomly from all the side chain monomers, and the part of the side chain from the selected monomer to the free end of the side chain is transformed by one of the 48 symmetry operations.

The initial configuration in the simulation is constructed by taking the backbone as a rod, choosing all backbone bond vectors of length $\ell_b = 3$ and oriented in the z-direction. The bond vectors of the side chain are chosen randomly from one of the allowed bond vectors in the (xy)-plane, growing the side chains step

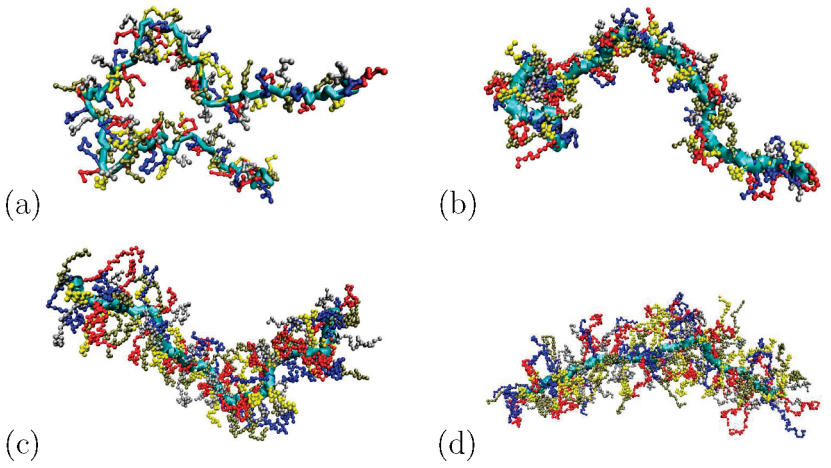

Figure 2. Snapshots of the conformations of bottle-brush polymers with $N_b = 131$ monomers on the backbone and with side chain lengths (a) $N = 6$, (b) $N = 12$, (c) $N = 24$, and (d) $N = 48$.

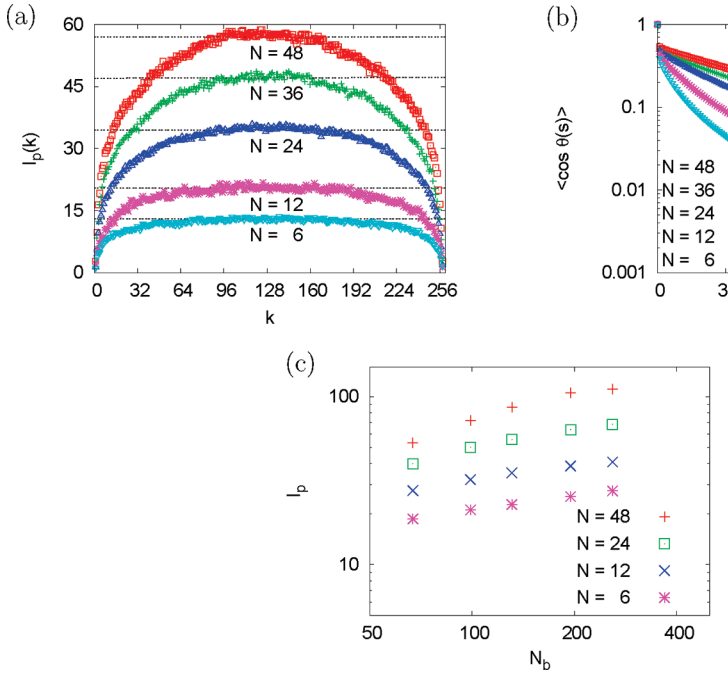

Figure 3. (a) Projection of the end-to-end vector of the backbone of the bottle-brush onto the local bond orientation, plotted vs the index k labeling the monomers along the backbone, for $N_b = 259$ and side chain lengths $N = 6$, 12, 24, 36, and 48 (from bottom to top). Dotted horizontal straight lines indicate estimates $\ell_p^{(1)}$ of the persistence length. (b) Bond vector correlation function $\langle \cos \theta(s) \rangle$ of the backbone {eq 17} plotted against the "chemical distance" along the backbone s in a semilog scale for $N_b = 259$ and various values of N, as indicated. (c) Persistence length $\ell_p = (\ell_p^{(1)} + \ell_p^{(2)})/2$ plotted vs N_b, for four different choices of N.

by step from the grafting site, and obeying excluded volume constraints. Then equilibration is achieved by N_{tot} "L 26" moves. After reaching equilibrium, averages are taken in a run where a Monte Carlo step is a sequence of N_{tot} "L 26" moves, k_{pb} pivot moves of the backbone and k_{pc} pivot moves of side chains; k_{pb} is chosen such that the acceptance ratio is about 40%, while $k_{pc} = n_c/4$. In order to check that equilibrium is actually reached, auto-correlation functions of the mean square radii of gyration of both side chains and the backbone are monitored. Figure 2 shows typical snapshots of equilibrated conformations of bottle-brushes with $N_b = 131$. One can see already directly from the snapshots that the bottle-brush polymers under good solvent conditions are not like flexible long cylinders, the side chain monomers are not at all densely packed around the backbone. At the same time, the snapshots already suggest a clear stiffening of the backbone with increasing chain length of the side chains. This stiffening effect can be made quantitative by the concept of the persistence length.[50−52]

There are several prescriptions of how to obtain this persistence length from an ensemble of configurations of the chain. One definition uses the projection of the end-to-end vector of the chain (forming the backbone) onto the unit bond vectors of bond k measured in terms of the average length of this bond

$$\ell_p(k) = \langle \vec{b}_k \cdot \vec{R}_{b,e} / |\vec{b}_k|^2 \rangle \tag{16}$$

In a plot of $\ell_p(k)$ as a function of the index k labeling the monomers along the backbone one finds a central plateau (Figure 3a). The height of this plateau can be taken as a definition, $\ell_p^{(1)}$, of the persistence length. Alternatively, one may consider the orientational correlation function of unit vectors $\vec{e}_k$ along the bond vector $\vec{b}_k$,

$$\langle \cos \theta(s) \rangle = \frac{1}{N_b - 1 - s} \left\langle \sum_{k=1}^{N_b - 1 - s} e_k \cdot e_{k+s} \right\rangle \tag{17}$$

Ideally, this function shows an exponential decay ($\exp(-s/\ell_p^{(2)})$) and indeed the data (Figure 3b) are compatible with this expectation, but only for large enough s. To avoid ambiguities due to the problem where the exponential decay begins, we have used the definition (implying $N_b \to \infty$ and assuming the $\ell_p^{(2)}$ stays well-defined in this limit; in practice the integration over s was a summation extended over discrete values from $s = 1$ up to $s = N_b - 1$)

$$\ell_p^{(2)} = b \int_0^\infty \langle \cos \theta(s) \rangle \, \mathrm{d}s \tag{18}$$

where a prefactor b has been used to account for the fast decay at small s. For the case of interest in Figure 1, $N_b = 259$, we obtain $\ell_p^{(1)} \approx 57$ and $\ell_p^{(2)} \approx 54$ (in units of the number of backbone bonds). Using the translation to a physical length scale quoted in Figure 1a, this would translate to persistence lengths of about 40 nm (note that $\ell_b \approx 2.7$ lattice spacings in our model), quite comparable to the estimate quoted by Rathgeber et al.[9]

However, the fact that for small side chain lengths N there is a long-range of s where the exponential decay of $\langle \cos \theta(s) \rangle$ with s does not yet hold is disturbing, as well as the need to introduce the factor b to approximately compensate for the initial fast decrease. These problems with the proper choice of a definition of the persistence length were also noted by Yethiraj.[40] Even more problematic is the fact that the definition due to Flory,[50,64] eq 16, has such a pronounced variation with k and actually the widths of the "plateaus" which we have used for obtaining the estimates $\ell_p^{(1)}$ indicated by the horizontal broken straight lines in Figure 3a are relatively short in comparison with N_b. If we would, alternatively, define a third estimate as an average,

$$\ell_p^{(3)} = (1/N_b) \sum_{k=1}^{N_b} \ell_p(k) \tag{19}$$

we would obtain an estimate which is systematically smaller (roughly $\ell_p^{(3)} \approx (2/3)\ell_p^{(1)}$).

Actually, the fact that is quite evident from Figure 3a, namely that there is no constant local persistence $\ell_p^{(k)}$ over some extended region of k in the interior of a bottle-brush polymer under good solvent conditions, points toward a more fundamental problem of polymer science: In good solvents, due to long-range orientational correlations along the polymer chain, the persistence length is NOT a well-defined characteristic of a polymer chain, that is independent of its chain length.[65,66] Schäfer et al.[65,66] showed by renormalization group methods for a linear chain with N_b monomers that in the limit $N_b \to \infty$ one has a simple scaling result for $\ell_p(k)$, apart from a prefactor a,

$$\ell_p(k) \approx a \left[\left(\frac{k(N_b - k)}{N_b} \right) \right]^{2\nu - 1} \tag{20}$$

which implies that $\ell_p^{(1)} \propto N_b^{2\nu-1} \approx N_b^{0.176} \to \infty$. Of course, for a bottle-brush eq 20 holds as well, and the length a appearing in the prefactor in eq 20 will depend on the side-chain length N.

Of course, at the Θ temperature (where $\nu = {}^1/_2$), eq 20 no longer is applicable, due to the tricritical character of the scaling behavior at $T = \Theta$, where logarithmic corrections to the leading power laws are predicted. In the excluded volume case, however, the standard notion that one finds in the textbooks[67] "The persistence length is a constant for each given polymer. This constant is the basic characteristic of polymer flexibility" (ref 67, p 5) does not apply; this notion only applies for strictly ideal chains. Even in dense melts[60] or at the Θ temperature[68] care is necessary, since $\langle \cos \theta(s) \rangle \propto \exp(-s/\ell_p)$ does not hold there either, but rather $\langle \cos \theta(s) \rangle \propto s^{-3/2}$, at least implying that eq 18 for $N_b \to \infty$ converges.

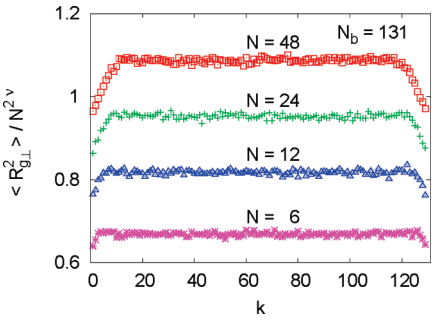

Figure 4. Rescaled mean-square gyration radius in perpendicular direction, plotted vs the side chain label k, for $N_b = 131$ and 4 side chain lengths, as indicated.

It appears that these basic conceptual problems what a persistence length means, and on what quantities it depends, have not been addressed in the experimental literature on bottle-brushes at all. Connolly et al.[39] obtain data similar to Figure 3a but study only one (small: $N_b = 48$) value of the backbone chain length. Figure 3c presents a plot of the persistence lengths, as extracted from the definitions eqs 16, 18 in our study, vs N_b, to demonstrate that this dependence of the persistence length on backbone chain length N_b, for bottle-brush polymers is a significant problem, irrespective of the side chain length N. In view of Figure 3c, we feel that the discussion of measured persistence lengths for bottle-brushes in the experimental literature needs reconsideration.

Next we turn to the mean square gyration radius $\langle R_{g,\perp}{}^2 \rangle$ of the side chains in perpendicular direction to the orientation of the backbone at the grafting site (Figure 4). One finds that the increase of $\langle R_{g,\perp}{}^2 \rangle$ with N exceeds the simple excluded volume power law in $d = 3$ dimensions, $\langle R_{g,\perp}{}^2 \rangle \propto N^{2\nu}$, only slightly, no evidence for the strong stretching behavior (eq 2) is found, as noted in ref 41 for a different model.

In Figure 4, we present the gyration radii $\langle R_{g,\perp}{}^2 \rangle / N^{2\nu}$ as a function of the index k where the side chains are grafted along the backbone. One sees that the radii are systematically smaller near the backbone ends (because there the side chains have more space, and the average orientation of their end-to-end vector is not perpendicular to the backbone,[43] unlike the inner parts of the chain). However, in this case, a very well-defined quite flat plateau in the plots vs k is reached, at first glance already very different from $\ell_p(k)$ (Figure 3a). We have also checked that these plateaus (for large N_b) are completely independent of N_b as expected.[63]

Both for a correct estimation of such chain linear dimensions where we resolve directions perpendicular and parallel to the backbone and for the estimation of the monomer radial density profile $\rho(r)$, one needs to properly take into account that the backbone of the bottle-brush is not straight but rather an undulating line.[49] Hsu et al.[49] recently suggested to solve this problem by cutting a bottle-brush polymer into $n_s = N_b/\ell_c$ sections (Figure 5). Evidence has been presented[49] that the optimum choice for ℓ_c is of the order of the persistence length ℓ_p, but fortunately the results are not sensitive to the precise value chosen for ℓ_c at all. It was also shown[49] that in the parameter range of interest there is not much difference between $\rho(r)$ for bottle-brushes with flexible backbones and their counterparts with rigid backbones.

Figure 6 gives then a plot of $\rho(r)$ vs r, combining the data for four side chain lengths ($N = 6$, 12, 24 and 48) and three backbone lengths, $N_b = 67$, 131, and 259. It is also shown that eq 8 provides a good fit of $\rho(r)$, similar as in the case of bottle-brushes with rigid backbones. If one uses instead the same type of function to fit the cross-sectional structure factor $S_{cs}(q)$, treating eq 10 as a definition of $S_{cs}(q)$ rather than as an approximation, and using the fact

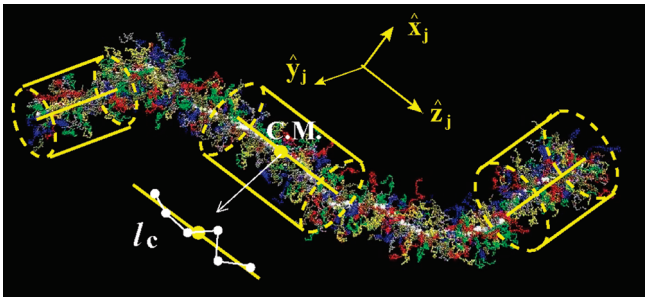

Figure 5. Snapshot of a bottle-brush polymer, simulated using the bond fluctuation model for the case $N_b = 387$, $N = 48$, $\sigma = 1$, and indicating the definition of the local coordinate system. One segment of the backbone consisting of ℓ_c bonds is plotted next to the chain. Cylinders surrounding the simulated chain show how the local orientation of these coordinate systems changes.

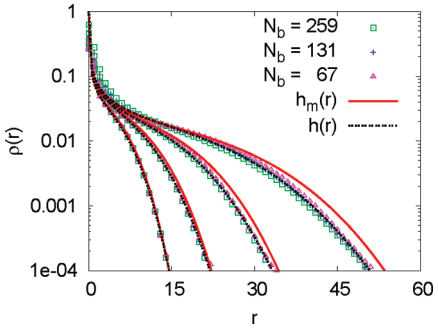

Figure 6. Radial distribution function $\rho(r)$ plotted vs r for backbone lengths $N_b = 67$, 131, and 259 (shown by different symbols), and for side chain lengths $N = 6$, 12, 24, and 48 from left to right. Fitting function $h(r)$ is given in eq 8, parameters describing the best fit are quoted in Table 1. Fitting function $h_m(r)$ is also given by eq 8, but parameters were chosen to reproduce the cross-sectional structure factors shown in Figure 7b in the regime of the respective maximum.

Table 1. Fitting Parameters r_1, r_2, and x of Fitting Functions $h(r)$ and $h_m(r)$ (eq 8) for Bottle-Brush Polymers of Side Chain Lengths $N = 6$, 12, 24, and 48

		$N = 6$	$N = 12$	$N = 24$	$N = 48$
$h(r)$	r_1	0.022	0.029	0.030	0.034
	r_2	7.95	12.0	19.0	30.3
	x	2.65	2.63	2.75	2.77
$h_m(r)$	r_1	0.023	0.029	0.030	0.032
	r_2	8.19	12.8	20.9	34.0
	x	2.80	2.88	3.08	3.25

that in the simulation $S_b(q)$ can be found independently without the need of any assumptions such as eq 12, see Figure 7, one obtains a slight but systematic overestimation of the profile (Figure 6). More details on both the simulation technique and specific results will be presented elsewhere.[63]

3. Comparison Between Experiment and Simulation

Here we focus on the comparison of our simulations exclusively with the scattering data of Rathgeber et al.,[9,10] since this work presented accurate structure factors $S(q)$ over a wide range of q, extending over more than two decades in wavenumber, $0.005\ \text{nm}^{-1} \le q \le 1.8\ \text{nm}^{-1}$, varying both the backbone length and the side chain length of their bottle-brush polymers. For the backbone polymer, hydroxyethyl methacrylate (PMMA) was used, with flexible poly(*n*-butyl acrylate) (PnBA) as side chains, using toluene as a solvent which is a good solvent for both polymers. Backbone chain lengths were chosen as $N_b^{\text{exp}} = 188$, 400, and 780, respectively, side chain lengths being in the range from $N = 22$ to $N = 98$. Note, however, that some experimental uncertainty due to polydispersity always is inevitable (for the main chain the molecular weight ratio M_w/M_n typically is in the range[9] $1.1 \le M_w/M_n \le 1.3$). For details on the synthesis of the samples, chemical characterization and experimental procedures we refer to ref 9, where all data that are discussed here were first published. The wide range of q was achieved by combining static light scattering with small angle neutron scattering techniques.

In fact, already in ref 10, a qualitative comparison with Monte Carlo simulations of bottle-brushes was performed, and an encouraging similarity was noted. In this latter work, however, only a very restrictive set of parameters was explored (for $N_b = 100$ and $N_b = 200$ side chain lengths were $N = 5$, 10, and 20), and hence no quantitative mapping between simulation and experiment could be attempted. Also, no information on $\rho(r)$ could be given.

When one considers an explicit mapping of a coarse-grained model of a flexible linear polymer and a real material, one must keep in mind that the self-similar character of the conformation of the chains allow for some arbitrariness of the scales chosen for this mapping. E.g, when one considers dense melts, where chains (with respect to mean-square distances) obey Gaussian statistics, one may combine s subsequent monomers of a chain having N monomers in total into an effective unit, so that $n = N/s$ effective units per chain occur. Requiring that the end-to-end distance stays invariant, we have $\langle R_e^2 \rangle = C_\infty \ell_b^{(2)} N = \ell^2 n$, C_∞ being the characteristic ratio and ℓ the distance between the effective units. Obviously, this mapping has a solution, namely $\ell^2 = C_\infty \ell_b^2 s$, irrespective of the precise choice of s. However, when one requires that the thickness of the polymer chain is retained in the mapping one obtains s not very much larger than unity (typically $s = 3-5$). E.g., in their mapping of polyethylene melts to the bond fluctuations model, Tries et al.[69] translated $s = 5$ subsequent C−C bonds into one bond vector of the bond fluctuation model. From this mapping, a correspondence of one lattice unit to about 2 Å was derived.[69]

A similar arbitrariness in the translation between experimental (N^{exp}) and simulation (N) chain lengths exists in the good solvent case, of course, when just isolated single chains are considered. However, for bottle-brush polymers the situation is less clear, since different local stiffness of the backbone polymer (without side chains attached) and of the side chains may give rise to somewhat different factors relating N_b^{exp} to N_b and N^{exp} to N (see Figure 1). However, there exists only a single factor relating the length scale of the simulation model to the real length scale. Since the mapping should conserve the chain architecture (i.e., the model should have about the same number of side chains as the real bottle-brush polymer), it is a nontrivial issue whether an accurate mapping is at all possible or not. Needless to say, even for an accurate mapping such as shown in Figure 1 one cannot expect that the lattice describes the real monomer packing on the subnanometer scale: only on the scale of several lattice spacings, corresponding to one nm or more, one can expect the coarse-grained model to yield an accurate description. Therefore, it is not surprising that the perfect agreement between experiment and simulation, demonstrated for $S(q)$ in Figure 1 for two examples, is restricted to special cases; in other cases additional choices of simulation parameters would be needed to obtain a similar agreement. As an example, Figure 8 presents the experimental structure factor for the choice $N_b^{\text{exp}} = 400$, $N^{\text{exp}} = 22$. Since in Figure 1a we have already seen that $N_b^{\text{exp}} = 400$ can be fitted by $N_b = 259$ (and $N^{\text{exp}} = 62$ translates into $N = 48$), we expect that again $N_b = 259$ should provide the best fit, and N should be in the range of $15 \le N \le 18$. Therefore, Figure 8 includes simulation data for $N = 12$ and $N = 24$, and indeed we see that the curves for $N_b = 259$ are closest to the experimental data, and while near $q \approx 0.5\ [\text{nm}]^{-1}$ the simulation curve $N = 12$ slightly overestimates the

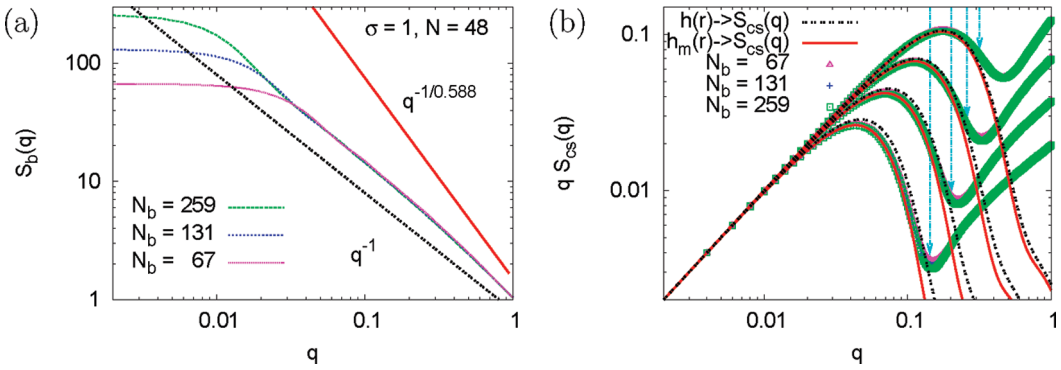

Figure 7. (a) Log−log plot of the structure factor $S_b(q)$ of the backbone monomers only plotted vs q for the case of side chain length $N = 48$ and three choices of backbone chain length, as indicated; straight lines show the power law $S_b(q) \propto q^{-1}$ (for a straight rod), $S_b(q) \propto q^{-1/\nu}$ (for a self-avoiding walk), respectively. (b) Cross-sectional structure factor $S_{cs}(q)$ defined as the ratio $S(q)/S_b(q)$, multiplied by q and shown as log−log plot vs q, for three choices of the backbone chain length N_b as shown, and four choices of side chain length, $N = 6$, 12, 24, and 48 (from left to right). Curves show predictions obtained from $h(r)$ in Figure 6 or fit to $h_m(r)$, respectively (only the region for q smaller than the values indicated by the vertical errors being fitted).

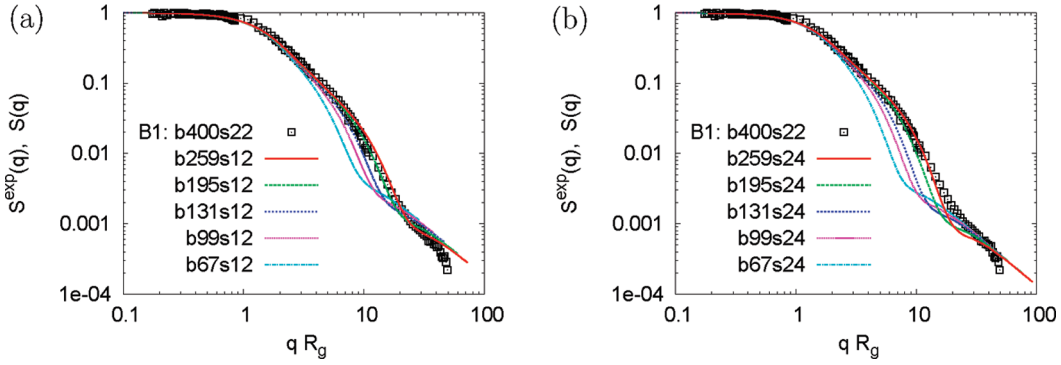

Figure 8. Normalized structure factor $S^{exp}(q)$ plotted vs qR_g for the sample with $N_b^{exp} = 400$, $N^{exp} = 22$, compared with simulated structure factors $S(q)$ for $N = 12$ (a) and $N = 24$ (b). Different backbone lengths $N_b = 67$, 99, 131, 195, and 295 are shown, as indicated.

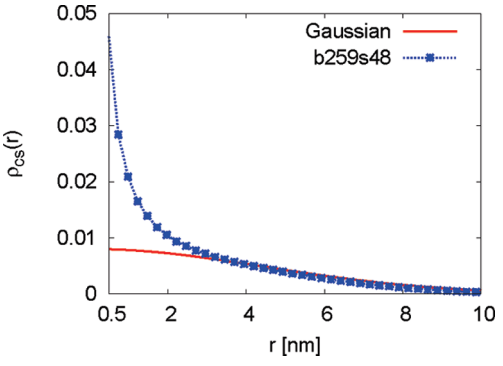

Figure 9. Radial density distribution of the monomers, $\rho(r)$, plotted vs r, for the simulated system with $N_b = 259$, $N = 48$, compared to the experimental system of Figure 1a, with $N_b^{exp} = 400$, $N^{exp} = 62$, and showing the assumed[9] Gaussian profile, eq 4, with the experimental cross-sectional gyration radius of 6.30 nm. The simulation yields a value $R_{g,cs} = 5.04$ nm.

data, the simulation curve for $N = 24$ slightly underestimates them. As expected, all other simulation curves are clearly off the data. This approximate transferability of the mapping between simulation and experiment between different cases indicates that agreements as demonstrated in Figure 1 are not just a mere accident.

Having established an approximate correspondence between experiment and simulation in specific cases, we can compare additional properties explicitly on physical scales, using the length rescaling factor quoted in Figure 1. As an example, Figure 9 compares the radial monomer density profile, that one can extract from the simulation directly and accurately[49,63] with the prediction from experiment,[9] where a rather complicated fitting procedure of the total structure factor $S(q)$, based on the approximation eqs 10−12 and further assumptions on the nature of the crossover function $\chi(q)$ in eq 12 are necessary,[9,55] as well as on the functional form of the profile, such as eq 4, 7, or 8 for instance. From such a simultaneous fitting procedure, involving several adjustable parameters, Rathgeber et al.[9] obtained $\langle R_{g,cs}^2 \rangle^{1/2} \approx 6.3$ nm for the case $N_b^{exp} = 400$, $N^{exp} = 62$ shown in Figure 1a. Using this value to predict $\rho(r)$ with the simple Gaussian profile eq 4, one notes that the Gaussian profile underestimates the actual density close to the backbone ($r \leq 2$ nm), but it is rather close to the actual profile in the range 2 nm $< r <$ 10 nm, which in view of the inevitable uncertainties involving a multiparameter fit is quite satisfactory. The doubts raised by Zhang et al.[11] about the validity of this analysis of Rathgeber et al.[9] are thus removed by the present reanalysis, as far as $\langle R_{g,cs}^2 \rangle$ is concerned. As a caveat, we recall that the lattice model provides a coarse-grained description of the polymer only, and hence the small-scale details of the density profile (for $r < 1$ nm) are not necessarily realistic. Furthermore, we want to point out that in ref 9 for the density profile also a power-law decay was tested. For sufficiently long side chains this function did not lead to any improvement of the fit compared to results obtained using a Gaussian profile. Therefore, we conclude that the deviations between the profiles at small length scales are irrelevant for the evaluation of the experimental data. At these length scales local density fluctuations dominate the scattering which are not considered in eq 12.

However, a real disagreement between the analysis of ref 9 and the present results based on simulation is found when one studies the persistence length (Figure 10); however, as a caveat, we recall

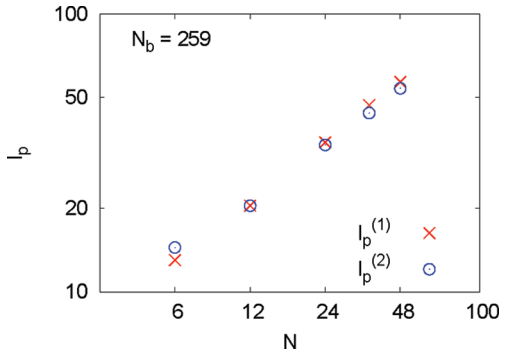

Figure 10. Log−log plot of the persistence lengths $\ell_p^{(1)}$, $\ell_p^{(2)}$ versus N, for the case $N_b = 259$. As units for ℓ_p the number of backbone bonds were chosen.

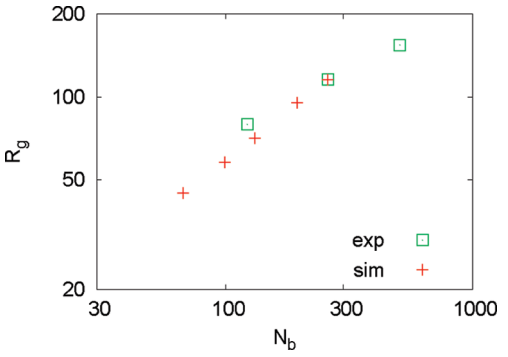

Figure 11. Log−log plots of the total gyration radius R_g vs N_b for $N = 48$. All lengths are quoted in units of lattice spacings. For comparison, the experimental data of Rathgeber et al.[9] are included, using for all data the conversion (Figure 1) that $N_b^{exp} = 400$ can be mapped to $N_b = 259$, $N^{exp} = 62$ can be mapped to $N = 48$, and one lattice spacing corresponds to 0.26 nm.

the ambiguities in the unique definition of the persistence length as a property characterizing chain stiffness under good solvent conditions, noted in the previous section. We find that the persistence length extracted from the plateau values in Figure 3a increases from $\ell_p \approx 13$ to about $\ell_p \approx 57$ backbone bonds, for $N_b = 259$. Since according to our mapping of length scales (Figure 1a) for this case (the length of a backbone bond is close to 3 lattice spacings) this means that the persistence length increases from about 9 nm to about 41 nm, and this increase is somewhat slower than linear in N. In contrast, the analysis of the experimental results using the Pedersen-Schurtenberger model yields a persistence length of 35 nm, independent of N^{exp} in the range $22 \leq N^{exp} \leq 98$. Recalling that for the case shown in Figure 1a the total gyration radius of the bottle-brush polymer is only 30.5 nm, this estimate[9] would imply that ℓ_p exceeds $\langle R_{g,bb}^2 \rangle^{1/2}$ already somewhat. As it is well-known, measurements of persistence lengths that are of the same order as the gyration radius are notoriously difficult and, thus are not sensitive enough to find weak increase of ℓ_p with N^{exp}. One should also keep in mind that the experiment measures the persistence length of the overall bottle-brush whereas the simulation directly probes the persistence length of the backbone. In addition, this much weaker increase of ℓ_p with N^{exp} might be an effect of weaker excluded volume effects in the experimental system (see discussion below). Thus, the simulation results suggest for the samples studied in ref 9 that the experiment might not be sensitive enough to detect weak increase of ℓ_p with N^{exp} of the backbone but it can also be due to differences in excluded volume interaction. We note, however, that the increase of persistence length with chain length N, seen in our simulation (Figure 10), seriously disagrees with available predictions from analytical theories and scaling proposals.[17,24,25] In the good solvent regime, to which our simulation applies, Fredrickson[24] suggested (for a persistence length defined from the free energy cost of bending a cylindrical bottle-brush)

$$\ell_p \propto N^{1.875} \tag{21}$$

obviously, this result is in strong disagreement with our finding, but it is possible that this discrepancy means that our side chains are too short for scaling theories to be applicable. However, our data match the experimentally relevant range of side chain length.[9−14] We also recall that the validity of the available theories for the persistence length of bottle-brushes is doubtful, since these theories do not take into account that the persistence length, defined from the plateau of $\ell_p(k)$ or from the decay of $\langle \cos \theta(s) \rangle$, depends on the backbone length N_b and diverges as $N_b \to \infty$, under good solvent conditions, rather than converging to a value that is independent of N_b (cf. eq 20). A more detailed discussion of this problem will be given elsewhere.[63]

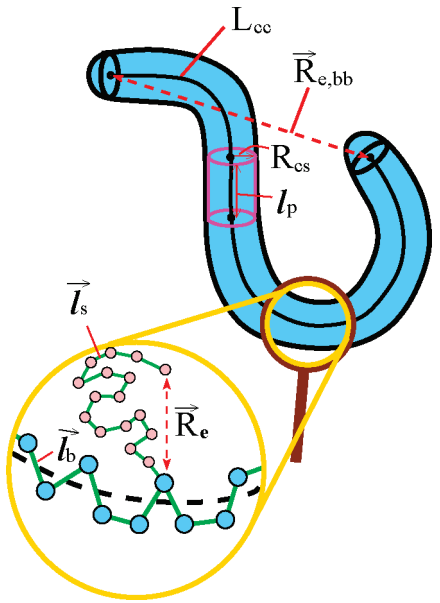

Figure 12. Coarse-grained description of a molecular bottle-brush as flexible spherocylinder (upper part) and a less coarse-grained description in terms of the main chain of N_b effective monomers, connected by bonds $\vec{l}_b$ forming the backbone, and side chains containing N effective monomers, connected by bonds $\vec{l}_s$ (lower part). Some characteristic lengths are shown: end-to-end vector $\vec{R}_e$ of a side chain and end-to end vector of the bottle-brush, $\vec{R}_{e,bb}$; length L_{cc} of the axis of the coarse-grained cylinder; persistence length ℓ_p and effective cross-sectional radius, R_{cs}.

Finally, we ask the question what happens when we use the conversion from the scales of the simulation to the scales of the experiment, as found in Figure 1a, namely the correspondence $N_b^{exp} = 400$ being mapped to $N = 259$ in the simulation, $N^{exp} = 62$ being mapped to $N = 48$ in the simulation, one lattice unit then being mapped to 0.26 nm, and use this conversion for a more complete comparison of the characteristics lengths? This question is answered in Figure 11, where the gyration radius is plotted vs N_b for $N = 48$, and the corresponding experimental data where N^{exp} was held constant (approximately) but the three choices $N_b^{exp} = 188$, 400, and 780 are included. The experimental value for the gyration radius for $N_b^{exp} = 400$ coincides with the value from the simulation by construction. One immediately recognizes from the log−log plot that both data sets are compatible with straight line variations on the log−log plot, implying a power law $\langle R_g^2 \rangle^{1/2} \propto N_b^{\nu_{eff}}$, but the slopes of the straight lines

(i.e., the value of the effective exponents ν_{eff}) differ, namely $\nu_{eff}(sim) \approx 0.71$ while $\nu_{eff}(exp) \approx 0.46$. The fact that in the experiment the variation of the gyration radius with N_b is so much weaker than in the simulation can be taken as indication that the effect of excluded volume in the simulation is very much stronger than in the experiment. In fact, the choice of the athermal bond fluctuation model means that the temperature T (as compared to the theta temperature Θ) is infinitely high! This is not true, of course, in the experiment, which is in the good solvent regime, but at a modest distance in temperature from the Θ temperature.

This difference also shows up when we compare the estimates of the persistence lengths from simulation and experiment, with respect to the side chain length variation. The simulation data vary approximately as $\ell_p \propto N^{0.3}$ while the increase of ℓ_p with N^{exp} is so small that in ref.[9] it was even suggested that ℓ_p might saturate for large N^{exp}. Again this much weaker increase is plausible as an effect of much weaker excluded volume effects. Note that the good agreement for $N^{exp} = 62$ ($N = 48$) is nontrivial, since the length scale conversion is no longer a fit parameter! However, we warn the reader that anyway the persistence length ℓ_p, according to its standard definitions, is an ill-defined property since it depends on the backbone length N_b (eq 20). This was already shown in Figure 3c. A backbone length independent measure of local chain stiffness would be provided by the length $\tilde{\ell}_p$ defined in eq 1.

4. Conclusions

In this paper, we have presented a comprehensive Monte Carlo simulation study of the conformation of flexible molecular bottle-brushes under good solvent conditions, and we have attempted a quantitative comparison with the experimental data,[9] based on the matching of the structure factor over a wide range of wave numbers. We have discussed the conformation of the molecular bottle-brush in terms of various characteristic length scales, summarized in Figure 12. On the mesoscopic scale, a bottle-brush polymer with densely grafted side chain may resemble a flexible long spherocylinder. The interesting global length scales then are the contour length L_{cc} on the coarse-grained scale, and the end-to-end distance $\vec{R}_{e,bb}$ of the bottle-brush, and its statistical mean square average, $\langle \vec{R}^2_{e,bb} \rangle$ as well as the associated gyration radius square, $\langle R^2_{g,bb} \rangle$. Of course, one needs also to know the cross sectional radius R_{cs} and also the persistence length ℓ_p defined in such a way that it describes over which distance the cylinder is approximately straight.

This coarse-grained view on the mesoscale (Figure 12, upper part) needs to be complemented by a view on a finer (but still possibly coarse-grained) scale (Figure 12, lower part). Backbone (effective) monomers a distance ℓ_b apart from each other, follow roughly the contour in the center of the cylinder (so $N_b \ell_b \geq L_{cc}$). For grafting density $\sigma = 1$, each monomer carries a side chain, where N monomers (at distances ℓ_s apart) form a chain molecule with end-to-end distance $\vec{R}_e$, and mean square gyration radius $\langle R_g^2 \rangle$. For the side chains, it is also of interest to distinguish components of these radii in the direction of the local cylindrical axis and perpendicular to it, and to study the monomer density profile in the direction perpendicular to the cylinder axis. Of course, it is important to recall that the coarse-grained cylinder in Figure 12 is not densely filled with monomers, but rather the density (in the excluded volume limit) decreases smoothly with increasing distance from the axis of the coarse-grained cylinder.

We have used the bond fluctuation model on the simple cubic lattice to model both the backbone chain and the side chain, varying N from $N = 6$ to $N = 48$, and N_b from $N_b = 67$ to $N_b = 259$. Making use of a specially developed,[63] very fast and efficient, simulation algorithm,[63] data for the mean square gyration radius of both the total bottle-brush polymer and of the side chains were obtained. With respect to the side chains, the information has been resolved with respect to the index of the anchoring point along the backbone, to elucidate possible end effects associated with the "sphere caps" at the ends of the cylinder (but these effects are rather small, as Figure 4 indicates). The persistence length estimate, however, is much more affected by the presence of free ends (and the finite length of the backbone), cf. Figure 3. Our results give clear evidence that in the good solvent case the persistence length (according to its standard definitions) diverges as $N_b \to \infty$. Guided by the persistence length, one can introduce, as Figures 5 and 12 suggest, a local cylindrical coordinate system and thus obtain reliable information on the radial monomer density profile (Figure 6).

Comparing the structure factors from the set of experiments of ref 9 and from the present simulation, Figures 1 and 8, we find a few cases where by adjusting a single parameter (the conversion factor from lattice spacings to nanometer) an almost perfect match is possible. Therefore, we are able to test the experimental prediction for the radial monomer density profile and the associate linear dimension R_{cs}, Figure 12, that follow rather indirectly in the experiment from a multiparameter-fitting procedure of the total structure factor $S(q)$, Figure 9. We find reasonable agreement in the range 2 nm $< r <$ 10 nm with the proposed Gaussian profile,[9] while for $r \leq 2$ nm the actual profile found very directly in the simulation predicts much larger densities. On the other hand, the persistence lengths, found in the simulation vary rather strongly with side chain length, in contrast to what was originally suggested for the experimental results,[9] on the basis of the fitting procedure. One should also recall that the standard notion of persistence lengths is well-defined only for Gaussian chains, but not for real chains with excluded volume interactions, and it is not clear that the persistence length extracted from the Pedersen−Schurtenberger[55] fitting functions can be identified with the standard persistence length as defined in the eqs 16−18 following the text books.[64,67] But we recall that the simulation treats the limit of very strong excluded volume, due to our use of an "athermal" model (corresponding to a solution where no thermal crossover to a Θ solution occurs), and part of the differences between experiment and simulation may simply be due to the fact that the experiment is done under conditions not very far away from the Θ point. We can also test the basic ingredients involved in the fitting procedure step by step: the decoupling approximation, eq 10, can be directly tested because both $S_b(q)$ (Figure 7a) and $S_{cs}(q)$ (defined from eq 11), from the observed $\rho(r)$ can be independently estimated (Figure 7b). As in the case of bottle-brushes with straight rigid backbones, the decoupling approximation, eqs 10 and 11 gives rise to some problems when it is used to analyze the present simulations, but this is probably not the main reason why the accuracy of some of the properties extracted from the multiparameter fit of the experimental data is hard to ascertain. Instead, we think that both the approximations made for $\rho(r)$ and for $S_b(q)$ and the decoupling approximation together give rise to inaccuracies which can be hard to control, because the estimates for $\langle R_{g,bb}{}^2 \rangle$, ℓ_p, R_{cs} are all strongly correlated with each other. In view of these problems, the almost quantitative agreement between the various characteristic lengths extracted from the simulations with the corresponding experimental results is very satisfactory. Significant deviations between simulation and experiment are only found for the radial density profile on length scales where the scattering results are dominated by local concentration fluctuations (here $\leq$2 nm). These deviations are however not relevant for the quantities derived on larger length scales (R_g, ℓ_p, and R_{cs}).

We also confirm the finding of the experiments and of previous simulations that have shown that for the accessible side chain lengths scaling predictions are not (yet) useful.

Acknowledgment. This work was supported by the Deutsche Forschungsgemeinschaft (DFG), Sonderforschungsbereich SFB 625/A3 and by the European Science Foundation (ESF) under the STIPOMAT program. Extensive grants of computer time at the JUMP supercomputer of NIC Jülich and of the SOFTCOMP NoE computer cluster are acknowledged. S.R. is grateful to K. L. Beers and K. Matyjaszewski for the synthesis of bottle-brush polymers, and her special thanks go to T. Pakula for the fruitful collaboration,[9] in which the data were obtained that are reanalyzed here (Figures. 1, 8) and compared to computer simulation results.[10] We are also grateful to M. Schmidt for his stimulating critical comments.

References and Notes

(1) Advincula, R. C., Brittain, W. J., Caster, K. C., Rühe, J., Eds.; *Polymer Brushes*; Wiley-VCH: Weinheim, Germany, 2004.
(2) Zhang, F.; Müller, A. H. E. *J. Polym. Sci, Part A, Polym. Chem.* **2005**, *43*, 3461 [HIGHLIGHT: Cylindrical Polymer Brushes].
(3) Sheiko, S. S.; Sumerlin, B. S.; Matyjaszewski, K. *Prog. Polym. Sci.* **2008**, *33*, 759.
(4) Wintermantel, M.; Schmidt, M.; Tsukahara, Y.; Kajiwara, K.; Kohjiya, S. *Macromol. Chem. Rapid Commun.* **1994**, *15*, 279.
(5) Wintermantel, M.; Gerle, M.; Fischer, K.; Schmidt, M.; Wataoka, I.; Urakawa, H.; Kajiwara, K.; Tsukahara, Y. *Macromolecules* **1996**, *29*, 978.
(6) Kawaguchi, S.; Alaike, K.; Zhang, Z.-M.; Matsumoto, H.; Ito, K. *Polym. J.* **1998**, *30*, 1004.
(7) Beers, K. L.; Gaynor, S. G.; Matyjaszewski, K.; Sheiko, S. S.; Moller, M. *Macromolecules* **1998**, *31*, 9413.
(8) Lecommandoux, S.; Chièćot, F.; Borsali, R.; Schappacher, M.; Deffieux, A.; Brûlet, A.; Cotton, J. P. *Macromolecules* **2002**, *35*, 8878.
(9) Rathgeber, S.; Pakula, T.; Matyjaszewski, K.; Beers, K. L. *J. Chem. Phys.* **2005**, *122*, 124904.
(10) Rathgeber, S.; Pakula, T.; Wilk, A.; Matyjaszewski, K.; Lee, H.-I.; Beers, K. L. *Polymer* **2006**, *47*, 7318.
(11) Zhang, B.; Gröhn, F.; Pedersen, J. S.; Fischer, K.; Schmidt, M. *Macromolecules* **2006**, *39*, 8440.
(12) Gunari, N.; Schmidt, M.; Janshoff, A. *Macromolecules* **2006**, *39*, 2219.
(13) Feuz, L.; Strunz, P.; Geue, T.; Textor, M.; Borisov, O. *Eur. Phys. J. E* **2007**, *23*, 237.
(14) Bolisetty, S.; Airaud, C.; Xu, Y.; Müller, A. H. E.; Harnau, L.; Rosenfeldt, S.; Lindner, P.; Ballauff, M. *Phys. Rev. E* **2007**, *75*, 040803(R).
(15) Birshtein, T. M.; Zhulina, E. B. *Polymer* **1984**, *25*, 1453.
(16) Witten, T. A.; Pincus, P. A. *Macromolecules* **1986**, *19*, 2509.
(17) Birshtein, T. M.; Borisov, O. V.; Zhulina, E. B.; Khokhlov, A. R.; Yurasova, T. A. *Polym. Sci. USSR* **1987**, *29*, 1293.
(18) Wang, Z.-G.; Safran, S. A. *J. Chem. Phys.* **1988**, *89*, 5323.
(19) Ligoure, C.; Leibler, L. *Macromolecules* **1990**, *23*, 5044.
(20) Ball, R. C.; Marko, J. F.; Milner, S. T.; Witten, T. A. *Macromolecules* **1991**, *24*, 693.
(21) Murat, M.; Grest, G. S. *Macromolecules* **1991**, *24*, 704.
(22) Dan, N.; Tirrell, M. *Macromolecules* **1992**, *25*, 2890.
(23) Wijmans, C. M.; Zhulina, E. B. *Macromolecules* **1993**, *26*, 7214.
(24) Fredrickson, G. H. *Macromolecules* **1993**, *26*, 2825.
(25) Zhulina, E. B.; Vilgis, T. A. *Macromolecules* **1995**, *28*, 1008.
(26) Sevick, E. M. *Macromolecules* **1996**, *29*, 6952.
(27) Rouault, Y.; Borisov, O. V. *Macromolecules* **1996**, *29*, 2605.
(28) Saariaho, M.; Ikkala, O.; Szleifer, I.; Erukhimovich, I.; ten Brinke, G. *J. Chem. Phys.* **1997**, *107*, 3267.
(29) Saariaho, M.; Szleifer, I.; Ikkala, O.; ten Brinke, G. *Macromol. Theory Simul.* **1998**, *7*, 211.
(30) Rouault, Y. *Macromol. Theory Simul.* **1998**, *7*, 359.
(31) Saariaho, M.; Subbotin, A.; Szleifer, I.; Ikkala, O.; ten Brinke, G. *Macromolecules* **1999**, *32*, 4439.
(32) Shiokawa, K.; Itoh, K.; Nemoto, M. *J. Chem. Phys.* **1999**, *111*, 8165.
(33) Subbotin, A.; Saariaho, M.; Ikkala, O.; ten Brinke, G. *Macromolecules* **2000**, *33*, 3447.
(34) Khalatur, P. G.; Shirvanyanz, D. G.; Starovoitova, N. Y.; Khokhlov, A. R. *Macromol. Theory Simul.* **2000**, *9*, 141.
(35) Vasilevskaya, V. V.; Klochkov, A. A.; Khalatur, P. G.; Khokhlov, A. R.; ten Brinke, G. *Macromol. Theory Simul.* **2001**, *10*, 389.
(36) Denesyuk, N. A. *Phys. Rev. E* **2003**, *67*, 051803.
(37) Sheiko, S. S.; Borisov, O. V.; Prokhorova, S. A.; Möller, M. *Eur. Phys. J. E* **2004**, *13*, 125.
(38) Elli, S.; Ganazzoli, F.; Timoshenko, E. G.; Kuznetsov, Y. A.; Connolly, R. *J. Chem. Phys.* **2004**, *120*, 6257.
(39) Connolly, R.; Bellesia, G.; Timoshenko, E. G.; Kuznetsov, Y. A.; Elli, S.; Ganazzoli, F. *Macromolecules* **2005**, *38*, 5288.
(40) Yethiraj, A. *J. Chem. Phys.* **2006**, *125*, 204901.
(41) Hsu, H.-P.; Paul, W.; Binder, K. *Macromol. Theory Simul.* **2007**, *16*, 660.
(42) Hsu, H.-P.; Paul, W.; Binder, K. *Macromol. Symp.* **2007**, *252*, 58.
(43) Hsu, H.-P.; Paul, W.; Binder, K. *J. Chem. Phys.* **2008**, *129*, 204904.
(44) Qu, L.-J.; Jin, X.; Liao, Q. *Macromol. Theory Simul.* **2009**, *18*, 162.
(45) Stephan, T.; Muth, S.; Schmidt, M. *Macromolecules* **2002**, *35*, 9857.
(46) Li, C.; Gunari, N.; Fischer, K.; Janshoff, A.; Schmidt, M. *Angew. Chem., Int. Ed.* **2004**, *43*, 1101.
(47) Klein, J. *Proc. Inst. Mech. Eng. Part J* **2006**, *220*, 691.
(48) Klein, J. *Science* **2009**, *323*, 47.
(49) Hsu, H.-P.; Binder, K.; Paul, W. *Phys. Rev. Lett.* **2009**, *103*, 198301.
(50) Flory, P. J. *Principles of Polymer Chemistry*; Cornell University Press: Ithaca, NY, 1953.
(51) de Gennes, P. G. *Scaling Concepts in Polymer Physics*; Cornell University Press: Ithaca, NY, 1979.
(52) Des Cloizeaux, J.; Jannink, G. *Polymers in Solution, Their Modeling and Structure*; Clarendon Press: Oxford, U.K., 1990.
(53) Halperin, A.; *Soft Order in Physical Systems*; Rubin, Y.; Bruinsma, R., Eds. Plenum Press: New York, 1994; p 33.
(54) Kotlarchyk, M.; Chen, S. H. *J. Chem. Phys.* **1983**, *79*, 2461.
(55) Pedersen, J. S.; Schurtenberger, P. *Macromolecules* **1996**, *29*, 7602.
(56) Kratky, O.; Porod, G. *J. Colloid Sci.* **1949**, *4*, 35.
(57) Carmesin, I.; Kremer, K. *Macromolecules* **1988**, *21*, 2819.
(58) Deutsch, H. P.; Binder, K. *J. Chem. Phys.* **1991**, *94*, 2294.
(59) Paul, W.; Binder, K.; Heermann, D. W.; Kremer, K. *J. Phys. II* **1991**, *1*, 37.
(60) Wittmer, J. P.; Beckrich, P.; Meyer, H.; Cavallo, A.; Johner, A.; Baschnagel, J. *Phys. Rev. E* **2007**, *76*, 011803.
(61) Grassberger, P. *Phys. Rev. E* **1997**, *56*, 3682.
(62) Sokal, A. D. in *Monte Carlo and Molecular Dynamics Simulations in Polymer Science*; Binder, K., Ed.; Oxford Univ. Press: New York, 1995, p 47.
(63) Hsu, H.-P.; Paul, W.; Binder, K. Manuscript in preparation.
(64) Flory, P. J. *Statistical Mechanics of Chain Molecules*: Interscience: New York, 1969.
(65) Schäfer, L.; Ostendorf, A.; Hagar, J. *J. Phys. A* **1999**, *32*, 7875.
(66) Schäfer, L.; Elsner, K. *Eur. Phys. J. E* **2004**, *13*, 225.
(67) Grosberg, A. Yu.; Khokhlov, A. R. *Statistical Physics of Macromolecules*; AIP Press: New York 1994.
(68) Shirvanyants, D.; Panyukov, S.; Liao, Q.; Rubinstein, M. *Macromolecules* **2008**, *41*, 1475.
(69) Tries, V.; Paul, W.; Baschnagel, J.; Binder, K. *J. Chem. Phys.* **1997**, *106*, 738.